

Is breaking through matter a hot matter? A material failure prediction by monitoring creep

Tom Vincent-Dospital,^{1,2,*} Renaud Toussaint,^{1,2,†} Alain Cochard,¹ Eirik G. Flekkøy,² and Knut Jørgen Måløy²

¹*Université de Strasbourg, CNRS, IPGS UMR 7516, F-67000 Strasbourg, France*

²*SFF Porelab, The Njord Centre, Department of physics, University of Oslo, Norway*

(Dated: August 2, 2022)

In any domain involving some stressed solids, that is, from seismology to general engineering, the strength of matter is a paramount feature to understand. We here discuss the ability of a simple thermally activated sub-critical model, that includes the auto-induced thermal evolution of cracks tips, to predict the catastrophic failure of a vast range of materials. It is in particular shown that the intrinsic surface energy barrier, for breaking the atomic bonds of many solids, can be easily deduced from the slow creeping dynamics of a crack. This intrinsic barrier is however higher than the macroscopic load threshold at which brittle matter brutally fails, possibly as a result of thermal activation and of a thermal weakening mechanism. We propose a novel method to compute the macroscopic critical energy release rate of rupture, G_a , solely from monitoring slow creep, and show that this reproduces the experimental values within 50% accuracy over twenty different materials, and over more than four decades of fracture energy.

I. INTRODUCTION: FROM SLOW CREEP TO ABRUPT RUPTURE

Although seminal, the early theoretical descriptions of crack dynamics, such as Griffith's [1] or Slepian's [2, 3] one, was somewhat binary: beyond a critical mechanical load, matter suddenly breaks. It is however acknowledged that, at load levels below the critical one, a far slower crack propagation already occurs, that will here be referred to as 'creep'. This phenomenon was successfully modelled with Arrhenius-like sub-critical growth laws [4, 5], and is hence sometimes called 'stress corrosion'. With the increasing number of experimental work, the description of such a slow dynamics was quickly refined, and five propagation stages were notably distinguished [5]. Let us start this manuscript by summarising them. Figure 1 illustrates these stages in a V - G plot, where V is the crack velocity for a given load G , which is the 'energy release rate', that is the energy that the fracture consummates to advance by unit surface [1]. At stage 0, while under only a mild mechanical input, cracks do not actually propagate forward. This was notably explained by the existence of some healing processes, that there efficiently compete with the failure ones [4]. From this state, when the load is increased above a given threshold, some slow fracture growth starts to be observed (stage I). The propagation velocity V increases exponentially with the crack's energy release rate G . In a sub-critical (i.e., Arrhenius-like) description, it implies that V is to first order explained by an activation mechanism dependent on G , in a chemical-like rupture reaction [6]. Logically, this regime was observed to also depend on the surrounding temperature and on the fluid that is present in the fracture [7], which affects

the chemical reaction involved in molecular bond breaking. When reaching a faster propagation, some velocity plateau might then hold (stage II), possibly as the transport of fluid corrosive elements toward the tip can not efficiently cope with the crack advance. Such plateau is, in this case, only a transition to a sub-critical growth 'in-vacuum-condition', where the dynamics becomes notably insensitive to the fracture fluid (stage III). Finally, when a particular threshold is reached for the energy release rate, the velocity jumps to a far quicker regime: the material fails (stage IV). We will denote¹ this threshold G_a in J m^{-2} , with 'a' standing for 'avalanche'.

In this work, we will show how studying the slow creep regime allows to predict this particular failure load. This can lead to methods to characterise natural or lowly controlled materials, where the critical energy release rate G_a is not well known a priori, but where the monitoring of creep allows to infer it. In a previous study [8], we indeed proposed a unifying model of the slow creep and the fast regime, holding a precise quantification of the energy budget and the heating of the crack tip, that is coupled with an Arrhenius-type activation law. We have shown how it accounts, in some polymers [9], for seven decades of propagation velocities and for the transition, at the avalanche load, from creep to sudden failure. Here, we present how well this thermodynamics based model can predict the threshold G_a for a broad range of materials, by comparing its forecasts to actual experimental failure thresholds from twenty data sets from the literature. By doing so, one can actually identify the microscopic rup-

¹ This is usually referred to as G_c in experiments, since it corresponds to the value of the macroscopic energy release rate at which the velocity of fracture propagation jumps to much higher values. By contrast, in this article, we made the choice to design as G_c a microscopic property, and consequently use this different notation G_a for the the macroscopic (observable) critical energy release rate.

* vincentdospital@unistra.fr

† renaud.toussaint@unistra.fr

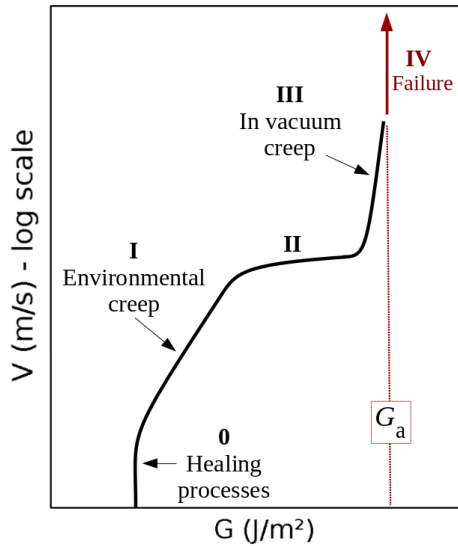


FIG. 1. Summary of the different forward crack velocity regions observed in experimental velocity curves. After *Fracture of Brittle Solids*, Lawn [5]

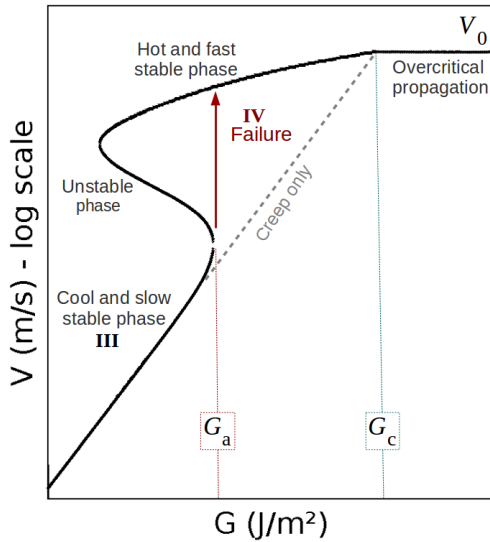


FIG. 2. Modelled crack velocity as a function of energy release rate, as per Eqs. (1) and (2). Stages I, III and IV correspond to the one labelled in Fig. 1. As explained in the text, stages 0 and II are here not covered. In our model, the failure occurs when the cracks becomes hot enough, that is, when $\Delta T \sim T_0$. The dashed line corresponds to a cold case $\Delta T \ll T_0$ in Eq. (1).

ture energy of the breaking bonds, G_c , and show how this quantity is related to, yet different from, the macroscopic G_a . The agreement between the predictions and the realisation is obtained for materials spanning more than 4 orders of magnitude in energy release rate, indicating the robustness of this description among different types of materials and the versatility of the theoretical framework.

II. THE THERMAL WEAKENING MODEL

We consider that the propagation of a crack follows an Arrhenius sub-critical growth law, in which the temperature term accounts for the induced heat generated at the plastic crack tip [10, 11]. Such a model, introduced in Refs. [8] and [9], writes as

$$V = V_0 \min \left[\exp \left(-\frac{d_0^3 (G_c - G)}{2lk_B(T_0 + \Delta T)} \right), 1 \right] \quad (1)$$

$$\frac{\partial(\Delta T)}{\partial t} = \frac{\lambda}{C} \nabla^2(\Delta T) + \frac{\phi GV}{C\pi l^2} f, \quad (2)$$

where the first equation describes the Arrhenius growth (i.e., the term in brackets is a probability for the thermal bath to overcome an energy barrier), and the second one in the diffusion equation governing the thermal evolution around the crack front. Here, V_0 is a nominal atomic speed related to the collision frequency in the thermal bath, and should typically be comparable to the mechanical wave velocity of the studied media [2, 12]. The activation energy is modelled proportional to $(G_c - G)$, where G_c is the surface energy barrier to overcome in order to break atomic bonds. d_0^3 is the characteristic volume for the bonds ($d_0 \sim 1 \text{ \AA}$), k_B is the Boltzmann constant, T_0 the ambient temperature and ΔT any variation away from it at the crack tip. A percentage ϕ of the power consummated per unit of crack length GV is uniformly dissipated as heat over a zone of support function f and of radius l . This heating zone is a subset of the process zone (that is the full extent of plasticity around the tip), and we assume that it also constrains the stress level σ at the tip, as verified in Vincent-Dospital et al. [9]: $\sigma \sim \sqrt{GE/l}$ [5], where E is the materials Young's modulus. This assumption is the reason why l also intervenes in Eq. (1). In Eq. (2), T is the temperature field, its value at the crack tip being $T_0 + \Delta T$ in Eq. (1). Finally, the heat conductivity and volumetric heat capacity of the solid matrix are respectively denoted λ and C .

Note that it was shown [9, 13] that at low velocities (i.e., the creep velocities we are interested in), ΔT computed from Eq. (2) can, more simply, be approximated to

$$\Delta T \sim \frac{\phi GV}{\lambda}, \quad (3)$$

which does not depend on C or l , notably because if the crack advances slowly enough, the temperature elevation is constrained by the heat diffusion skin depth $\sqrt{\lambda l / (\pi C V)}$ rather than the size of the heat production zone, as the former is, in this case, big compared to the latter.

Approximating Eqs. (1) and (2) by their steady state solutions, two stable propagation branches are derived from this model [8], as shown in Fig. 2: a fast phase, which is obtained for a hot crack tip and corresponds to the catastrophic failure of matter, and a slow one corresponding

to the creep regime, when $\Delta T \ll T_0$. In between these two branches, a hysteresis situation holds with a third unstable phase. In this study, we are here mainly interested in the slow to fast regime transition (i.e., that leads to quick material failure).

When approaching this transition, the velocity deviates from its negligible heating asymptotic expression, which is a simple exponential increase with the load G :

$$\ln\left(\frac{V}{V_0}\right) \sim (G - G_c) \left[\frac{d_0^3}{2lk_B T_0} \right], \quad (4)$$

as the rise in temperature ΔT in Eq. (1) becomes comparable to the room temperature T_0 . The particular energy release rate G_a is then reached, at which $\partial V/\partial G \rightarrow +\infty$, and beyond which the crack can only avalanche to a velocity that is orders of magnitude higher (see Fig. 2). The matter suddenly snaps. As a result of thermal activation, G_a is actually less than the actual surface energy barrier for breaking bonds G_c .

Although rarely regarded today, such an importance of the auto-induced heat to explain brittleness was early developed [14–16]. These studies reckon that the dissipated energy favours failure by locally softening the material at the tip. Our model neglects such a softening effect and instead considers that the reaction rate for rupture is increased from the elevated temperature, only as understood by statistical physics. Of course, both views are not mutually exclusive. In both cases, the G value of interest (i.e., G_a) remains similar: the threshold for which ΔT significantly overcomes the thermal background, so that a quick avalanche can be generated.

III. MODEL PREDICTIONS VERSUS REPORTED FAILURES

Extensive fracturing experiments on numerous materials can be found in the literature. Hence, we can compare the model predictions of G_a to some experimentally reported avalanche thresholds, that are often referred to as ‘critical energy release rate’ or ‘material toughness’, although it does not correspond to what is here denoted G_c , that is an intrinsic (microscopic) medium property not directly measurable at lab scale.

Note that Eq. (1) does not account for all of the creep regimes summarized in Fig. 1, that one can meet with an experimental test, but displays a unique low velocity slope (i.e., from Eq. (4)). We have indeed discarded any healing processes, needed to explain stage 0, as they are beyond the topic of the current study. Such processes can however be included in the model [9]. We have also assumed no rate-limiting environmental factor, that is, no significant chemical interaction of the matrix with the fracture fluid (i.e., no stage I or II). We have hence restricted our comparison to experimental data to such a

case, although distinguishing it with certitude is not always straightforward. When available, we have notably used data sets of dry experiments or with lowly corrosive fracture fluids. Note however that, when some fluid-matrix interaction does take place, the model can still be somewhat applied, if failure is preceded by a unique slope (i.e., if it occurs before the slope break between stages I and II), or after it, once clearly having entered in regime III. In this case, the definition of the surface energy barrier G_c may slightly change: from an intrinsic strength of the solid to an equivalent strength under a given chemical environment.

To predict G_a , it is of course needed to know, for each material, the values of the model constitutive parameters. Although they are not many, most of these parameters are not usually considered, and are hence unknown. It is however possible to estimate their order of magnitude from known material properties, or to assess them from the slow (creep) part of the loading curve. We have first considered that V_0 is of the order the mechanical wave velocity. It could ideally be that of the Rayleigh waves [12], but it is often simpler to rather estimate the shear wave velocity of solids, $V_S \sim \sqrt{\mu/\rho}$, as the shear modulus μ and the density ρ of most materials are easily available. The heat conductivity λ is also known in most cases, and T_0 is nothing but the room temperature at which a given reported experiment took place. We assume the interatomic space d_0 to be 1 Å. While it could be two or three times bigger depending on the materials, which would have an order of magnitude effect on the term d_0^3 , this uncertainty would only impact the estimation of l , as the ratio d_0^3/l is here of importance. We indeed have to deduce l and G_c from the slope and intercept of the slow sub-critical growth, that is, from the two terms of Eq. (4) fitted to the experimental curves with the fit parameters a and b : $\ln(V) = a + bG$. This gives

$$l = \frac{d_0^3}{2bk_B T_0} \quad (5)$$

$$G_c = \frac{2k_B T_0}{d_0^3} [\ln(V_0) - a]. \quad (6)$$

This implies that we can predict G_a if relying on some creep observations, that can yet be at loads far below the failure threshold. The only remaining model parameter, the percentage ϕ of energy converted into heat is mostly unknown. While qualitative statements, such as larger ϕ in metals rather than, say, polymers, are tempting, we have here arbitrarily fixed this percentage to 50% in all materials, except for a couple of instances where we could estimate it [9, 13].

Note that, while the velocity is often reported in relation to the stress intensity factor K rather than the energy release rate G , we have here converted from one to the other with the following relation: $G \sim K^2/E$ [5] to derive a and b , and then l and G_c . Backwardly, with the here proposed method, we will thus predict the tough-

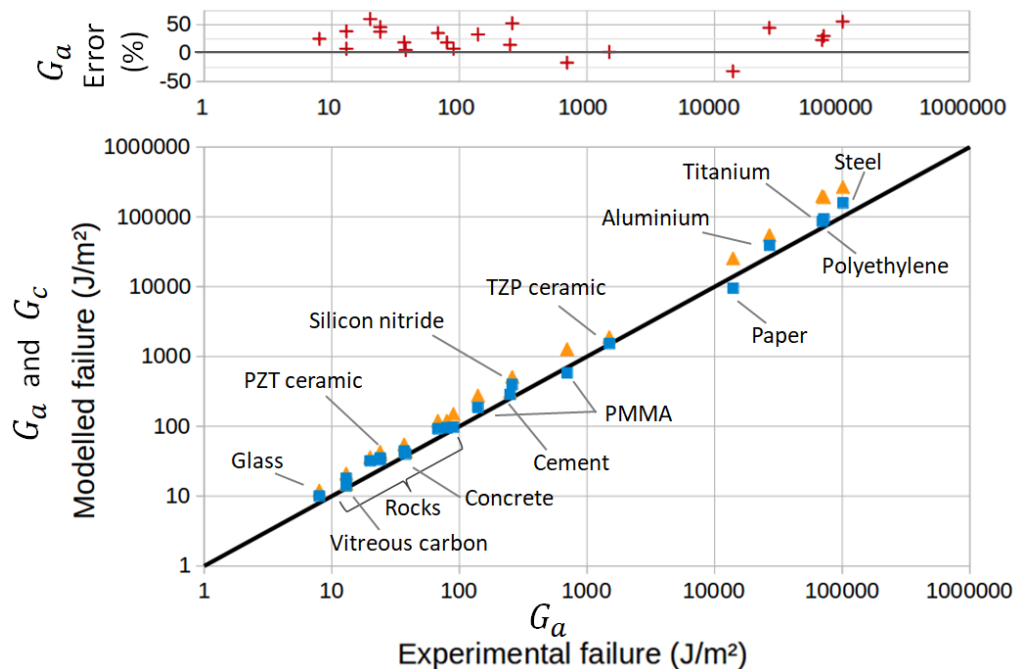


FIG. 3. (Bottom): Modelled G_a thresholds (squares) and modelled surface energy barrier G_c (triangles) compared to the experimental thresholds from the literature. The black line is the identity. The labels locate different materials. The unlabelled rock materials are quartz, sapphire, granite and andesite. See the supplementary material for an exhaustive list. (Top): Relative error on the avalanche threshold.

ness, $K_c \sim \sqrt{EG_a}$, based on the creep measurement. Indeed, all the introduced parameters can now be estimated, and we did so for twenty materials for which the creeping behaviour was studied in the literature [9, 17–34]. The corresponding G to V curves and the inferred parameters values are shown in the supplementary material. We can then solve the full two non linear equations (1) and (2), now taking into account the temperature rise ΔT . The inflection of this model, if it exists, where $\partial V/\partial G \rightarrow +\infty$ (see Fig. 2), can be identified as G_a and compared to the reported experimental thresholds. This comparison is summarised for all the media in Fig. 3, and our model displays there a good general description of catastrophic failure. In the same figure, the surface energy barrier G_c is also displayed for comparison, as well as the relative error made in the estimation of G_a .

IV. ANALYTICAL APPROXIMATION

While, to derive the modelled G_a , one should compute the full crack dynamics (i.e., as displayed in Fig. 2), and search for the points where $\partial G/\partial V = 0$, we explain in the supplementary material how Eqs. (1) and (2) also approximately lead to:

$$G_a \sim \frac{\lambda T_0}{\phi V_0} \frac{\exp(R_a)}{R_a}. \quad (7)$$

where R_a is the activation energy at the avalanche threshold counted in thermal energy units: $R_a = d_0^3(G_c - G_a)/(2lk_B T_0)$. As this ratio notably depends on G_a , Eq.(7) only implicitly defines the threshold. It however gives further insight on the influence of each parameter and, although a numerical solver is still required, it is simpler and far quicker than finding the accurate solution, and potentially easy to use in engineering applications. We show, in the supplementary material, how this approximation is a slight overestimation of the real solution, by about 0 to 10%.

V. MICROSCOPIC VS MACROSCOPIC FRACTURE ENERGY

In Fig. 3, one can notice that the surface energy barrier G_c is always similar in order of magnitude to the rupture threshold G_a . Yet, the rupture always occurs at a load less than G_c , with G_a being about twice lower in average for all the displayed solids. We have here explained how a weakening mechanism, as the thermal view that we have here developed, allows to account for this discrepancy. Having gathered various exponential creep data, and derived l and G_c from their slope and intercept in their $\ln V - G$ representations, we can notably infer the intrinsic crack energy barrier in each material: $U_c = d_0^3 G_c / (2l)$. As shown in Fig. 4, this quantity is always in the or-

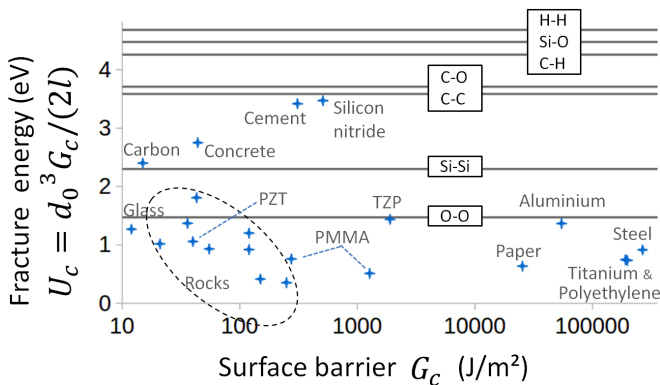


FIG. 4. Microscopic fracture energy $U_c = d_0^3 G_c / (2l)$ as a function of the macroscopic energy barrier G_c , for the same materials as Fig. 3. See the supplementary material for the exhaustive list. Note that the accuracy of U_c is not better than an order of magnitude. The horizontal lines show some typical covalent cohesion energies for comparison [35].

der of 10^{-19} J \sim 1 eV, logically comparable to the energy level that is necessary to unbind single atomic covalent bounds [35]. The actual values of U_c are yet often slightly inferior to the typical covalent strength. This could derive from an averaging effect, with cracks that are prone to follow the weakest paths, that possibly includes intermolecular bonds (such as Van der Waals and hydrogen links) and dislocations or atomic voids (i.e., when the distance between two consecutive breaking bonds is more than a few ångströms). For instance, in polymers, part of the rupture shall be inter-molecular, and, in rock-type materials, the crack dynamics might benefit from the intrinsic porosity. However, due to the simplicity of the model, care should be taken when interpreting U_c beyond its order of magnitude.

It is clear however that the value of G_c varies by a factor 10^4 for different materials, while its counterpart U_c does not. As most materials have the same U_c and d_0 , in order of magnitude, the large variability in G_c (and hence in G_a) that is observed is, in this description, attributable entirely to the variability in the scale for the release of heat. We indeed infer that l varies from the radius of a single atom, for the weakest materials, up to $1 \mu\text{m}$, for the ones with the highest G_c (see Fig. 5). The wider the plastic area that shields crack tips, the stronger is matter. But backwardly, we have discussed how the heat dissipation might be the root cause for dramatic ruptures in brittle solids, if the heat is not efficiently evacuated away from the rupture front.

We can compare the values of l with the more typical plastic radius predicted by a Dugdale view [36] of the process zone, $l_{\text{macro}} \sim G_c E / \sigma_y^2$, where σ_y is the tensile yield stress, beyond which macroscopic samples lose their elasticity. As shown in Fig. 5, the latter is consistently five to seven orders of magnitude higher than what we predict for l . This likely translates to the fact that plasticity (here understood as the dissipation of mechanical

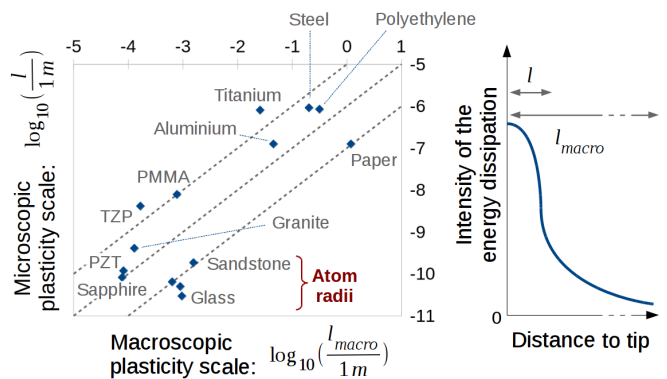


FIG. 5. (Left): Core size of the process zone l , as understood by our model, versus macroscopic plasticity scale l_{macro} , as derived from reported tensile yield stresses. The straight lines mark a factor 10^5 , 10^6 and 10^7 between both views. (Right): Simplified spacial distribution of the intensity (arbitrary unit) at which energy is dissipated (i.e., plasticity) around the crack tip, as a possible explanation for the difference in scale. The graph is not to scale as $l_{\text{macro}} \gg l$. The two unlabelled points in the vicinity of Glass represent Quartz and Concrete.

energy in any form) ought to be a rather heterogeneous phenomenon, with a greater density of energy dissipation close to the front than away from it. Thus, the scale of a process zone can be characterised either by its core radius l , where most of the heating due to the dissipation takes place, or by its full extent l_{macro} , where the rheology becomes non elastic. While the former is to include significant thermal losses, the latter can encompass various mechanisms, namely, the nucleation of dislocations, the release of residual heat over a greater volume, the emission of phonons and photons, or even some material change in phase.

Overall, Eq. (1) should be understood as:

$$V = V_0 \exp \left(- \frac{U_c - U(G^{[+]}, \text{plasticity}^{[-]})}{k_B T (\text{plasticity}^{[+]}, \text{diffusion}^{[-]})} \right), \quad (8)$$

where U is the mechanical energy corresponding to the stress actually transmitted to the crack tip covalent bond of average strength U_c , and where $[+]$ and $[-]$ indicate if the T and U functions are increasing or decreasing with the specified parameters.

VI. DISCUSSION AND CONCLUSION

We have thus presented a model that gives reasonable predictions of the rupture load, over a broad range of materials. We did this with a full expression (Eqs. (1) and (2)), or in simplified forms (Eqs. (1) and (3) or Eq. (7)). This predicted load is still, however, overestimated by about 25% (in average for all media, see the errors in Fig. 3). This could derive from numerous causes. First, most of our parameters were only broadly

estimated, when not arbitrarily fixed. We have in particular assumed that G_c is a homogeneously distributed constant, although it is likely to hold some level of quenched disorder [37, 38]. In this case, the overall creep dynamics (i.e. the slow branch of Fig. 2, described by Eq. (4)) would not be strongly affected, as it shall mainly depend on an average value of G_c . The failure, however, would be prone to occur on weaker locations [8], that are controlled by a lower G_c , which would explain our overestimation on G_a . It corresponds to the common idea that the overall strength of a material is highly dependent on its heterogeneities. Furthermore, the experimental error on the measurement of G_a could also be important, as the avalanches occur in a regime where the crack velocity diverges with G , just before test samples snap at a velocity comparable to that of the mechanical waves. Hence, the last mechanical load accurately measured before rupture is, by essence, to be slightly below the actual physical threshold. Note also that, sometimes, the actual creep stage (i.e., 0 to III in Fig. 1) that we fit to derive our parameters is not unambiguously identifiable on the experimental curves. Besides these considerations, the model is extremely simple, applying mesoscopic laws (i.e., Fourier conductivity and Arrhenius growth) at atomic scales. For instance, a propagative description [39] of the heat transport could be needed, due to the small time and space scales that are here considered. Overall, a transposition of the model into a, more complicated, atomistic solver [40] would be beneficial.

Still, the model we propose gave, in some instances [9], a comprehensive explanation of the full dynamics of failure. Additionally, we have here showed how G_c , the intrinsic surface energy barrier of materials, shall only depend on a heat dissipation scale around the crack tip, and that the accumulation of this induced heat is effectively reducing the mechanical resistance of matter ($G_a < G_c$).

Countering this latter effect could be a key to design advanced strong materials, in particular as some intriguingly tough solids such as graphene [41, 42] or arachnid silks [43], are indeed very conductive. Interestingly, the conductivity of spider threads even increases with deformation [43], which could be a nature made adaptive

defence mechanism for the stability of nets, whenever they are pressurized. Replicating such a behaviour with a man-made material would then be an important achievement that could lead to high performance cables or bulk materials. For instance, a first step could be the engineering of highly conductive atomic networks, integrated into strong solid matrices, thus limiting any local rise in temperature that could weaken the matter.

A more down-to-earth application of the model could be the monitoring of structures and infrastructures, as we have shown how their creep rate can be used to predict their failure. This would be of particular interest for bodies that have aged in uncontrolled conditions, in which the change in mechanical properties becomes uncertain with time, but could be inverted from their creep.

Finally, and although we have only treated about fracture in mode I, we suggest that most of the effects that we have discussed shall be valid for mixed-mode fracturing and solid friction. The latter is also suspected to hold some non negligible, thermal related, weakening mechanisms [44, 45], which could notably be a key in geophysics and in understanding the stability of seismic faults. In particular, when increasing the background temperature T_0 , it was shown that the model holds a critical point, beyond which not enough heat can be generated to trigger instabilities in the dynamics of cracks [8], which may physically explain the brittle-ductile transition in the Earth's crust [46, 47], below which rocks tend to flow rather than break.

ACKNOWLEDGEMENTS

The authors declare no competing financial interests in the publishing of this work and acknowledge the support of the IRP France-Norway D-FFRACT, of the Universities of Strasbourg and Oslo and of the CNRS INSU ALEAS program. We thank the Research Council of Norway through its Centres of Excellence funding scheme, project number 262644.

-
- [1] A. Griffith. The Phenomena of Rupture and Flow in Solids. *Philosophical Transactions of the Royal Society of London A: Mathematical, Physical and Engineering Sciences*, 221(582-593):163–198, January 1921. ISSN 1471-2962. doi:10.1098/rsta.1921.0006.
 - [2] L.I. Slepyan. Dynamics of a crack in a lattice. *Soviet Physics, Doklady*, 26:538–540, 1981.
 - [3] M. Marder. Slepyan's dynamic contribution to studies of fracture. *Philosophical Transactions of the Royal Society A: Mathematical, Physical and Engineering Sciences*, 2019.
 - [4] J.R. Rice. Thermodynamics of the quasi-static growth of Griffith cracks. *Journal of the Mechanics and Physics of Solids*, 26(2):61 – 78, 1978. doi:10.1016/0022-5096(78)90014-5.
 - [5] B. Lawn. *Fracture of Brittle Solids*. Cambridge Solid State Science Series. Cambridge University Press, 2 edition, 1993. doi:10.1017/CBO9780511623127.
 - [6] G. G. Hammes. *Principles of Chemical Kinetics*. Academic Press, 1978. ISBN 978-0-12-321950-3. doi:doi.org/10.1016/B978-0-12-321950-3.50005-0.

- [7] N. Brantut, M. J. Heap, P. G. Meredith, and P. Baud. Time-dependent cracking and brittle creep in crustal rocks: A review. *Journal of Structural Geology*, 52:17 – 43, 2013. ISSN 0191-8141. doi:10.1016/j.jsg.2013.03.007.
- [8] T. Vincent-Dospital, R. Toussaint, A. Cochard, K. J. Måløy, and E. G. Flekkøy. Thermal weakening of cracks and brittle-ductile transition of matter: A phase model. *Physical Review Materials*, 02 2020. doi:10.1103/PhysRevMaterials.4.023604.
- [9] T. Vincent-Dospital, R. Toussaint, S. Santucci, L. Vanel, D. Bonamy, L. Hattali, A. Cochard, K. J. Måløy, and E. G. Flekkøy. From thermal creeping to thermal weakening: How crushing plastic and unrolling tape unravels fracture physics. submitted, 2019. URL <https://arxiv.org/pdf/1905.07180.pdf>.
- [10] E. Orowan. Energy criteria of fracture. Technical report, Massachusetts Institute of Technology, Cambridge Department of Mechanical Engineering, 1954.
- [11] G. R. Irwin. Analysis of stresses and strains near the end of a crack traversing a plate. *Journal of Applied Mechanics*, 24:361–364, 1957.
- [12] L. B. Freund. Crack propagation in an elastic solid subjected to general loading. *Journal of the Mechanics and Physics of Solids*, 20(3):129 – 152, 1972. ISSN 0022-5096. doi:10.1016/0022-5096(72)90006-3.
- [13] R. Toussaint, O. Lengliné, S. Santucci, T. Vincent-Dospital, M. Naert-Guillot, and K. J. Måløy. How cracks are hot and cool: a burning issue for paper. *Soft Matter*, 12:5563–5571, 2016. doi:10.1039/C6SM00615A.
- [14] G. P. Marshall, L. H. Coutts, and J. G. Williams. Temperature effects in the fracture of PMMA. *Journal of Materials Science*, 9(9):1409–1419, Sep 1974. ISSN 1573-4803. doi:10.1007/BF00552926.
- [15] D. Maugis. Subcritical crack growth, surface energy, fracture toughness, stick-slip and embrittlement. *Journal of Materials Science*, 20(9):3041–3073, Sep 1985. ISSN 1573-4803.
- [16] G. Carbone and B. N. J. Persson. Hot cracks in rubber: Origin of the giant toughness of rubberlike materials. *Phys. Rev. Lett.*, 95:114301, Sep 2005. doi:10.1103/PhysRevLett.95.114301.
- [17] O. Lengliné, R. Toussaint, J. Schmittbuhl, J. E. Elkhoury, J. P. Ampuero, K. T. Tallakstad, S. Santucci, and K. J. Måløy. Average crack-front velocity during subcritical fracture propagation in a heterogeneous medium. *Phys. Rev. E*, 84:036104, Sep 2011. doi:10.1103/PhysRevE.84.036104.
- [18] S. Santucci. *Croissance lente thermiquement activée et piégeage d'une fissure dans les matériaux structurés à une échelle mésoscopique : expériences et modèles*. PhD thesis, Ecole normale supérieure de Lyon, www.theses.fr/2004ENSL0288, 2004.
- [19] M. Yoda, M. Nabetani, and W. Shim. Creep crack growth in polyethylene under combined mode I and mode II loading. *International Journal of Fracture*, 112(3):21–26, Dec 2001. ISSN 1573-2673. doi:10.1023/A:1022681718523.
- [20] S. M. Wiederhorn. Influence of water vapor on crack propagation in soda-lime glass. *Journal of the American Ceramic Society*, 50(8):407–414, 1967. doi:10.1111/j.1151-2916.1967.tb15145.x.
- [21] S.M. Wiederhorn and R.F. Jr. Krause. Crack growth in sapphire. In *Ceramic Engineering and Science Proceedings*, volume 23, pages 71–82. Wiley, 2002.
- [22] P. M. Dove. Geochemical controls on the kinetics of quartz fracture at subcritical tensile stresses. *Journal of Geophysical Research: Solid Earth*, 100(B11):22349–22359, 1995. doi:10.1029/95JB02155.
- [23] P.G. Meredith and B.K. Atkinson. Fracture toughness and subcritical crack growth during high-temperature tensile deformation of westerly granite and black gabbro. *Physics of the Earth and Planetary Interiors*, 39(1):33 – 51, 1985. ISSN 0031-9201. doi:10.1016/0031-9201(85)90113-X.
- [24] Y. Nara and K. Kaneko. Study of subcritical crack growth in andesite using the double torsion test. *International Journal of Rock Mechanics and Mining Sciences*, 42(4):521 – 530, 2005. ISSN 1365-1609. doi:10.1016/j.ijrmmms.2005.02.001.
- [25] J. Holder, J. E. Olson, and Z. Philip. Experimental determination of subcritical crack growth parameters in sedimentary rock. *Geophysical Research Letters*, 28(4):599–602, 2001. doi:10.1029/2000GL011918.
- [26] W. Wang, T. Tong, and Q. Yu. Subcritical crack growth induced by stress corrosion in hardened cement paste. In *9th International Conference on Fracture Mechanics of Concrete and Concrete Structures*. FraMCoS, 2016. doi:10.21012/FC9.177.
- [27] Y. Nara, M. Takada, D. Mori, H. Owada, T. Yoneda, and K. Kaneko. Subcritical crack growth and long-term strength in rock and cementitious material. *International Journal of Fracture*, 164(1):57–71, Jul 2010. ISSN 1573-2673. doi:10.1007/s10704-010-9455-z.
- [28] W. S. Oates, C. S. Lynch, D. C. Lupascu, A. B. K. Njiwa, E. Aulbach, and J. Rödel. Subcritical crack growth in lead zirconate titanate. *Journal of the American Ceramic Society*, 87(7):1362–1364, 2004. doi:10.1111/j.1151-2916.2004.tb07736.x.
- [29] J. Chevalier, C. Olagnon, and G. Fantozzi. Subcritical crack propagation in 3Y-TZP ceramics: Static and cyclic fatigue. *Journal of the American Ceramic Society*, 82(11):3129–3138, 1999. doi:10.1111/j.1151-2916.1999.tb02213.x.
- [30] A. G. Evans and S. M. Wiederhorn. Crack propagation and failure prediction in silicon nitride at elevated temperatures. *Journal of Materials Science*, 9(2):270–278, Feb 1974. ISSN 1573-4803. doi:10.1007/BF00550951.
- [31] G. Hénaff, G. Odemer, and B. Journet. Creep and creep-fatigue crack growth in aluminium alloys. In *Aluminium Alloys, Theory and Applications*, pages 259–282. IntechOpen, 2011. doi:10.5772/15153.
- [32] J. H. Huang and C. J. Altstetter. Internal hydrogen-induced subcritical crack growth in austenitic stainless steels. *Metallurgical Transactions A*, 22(11):2605–2618, Nov 1991. ISSN 1543-1940. doi:10.1007/BF02851354.
- [33] S. M. L. Sastry, R. J. Lederich, and B. B. Rath. Subcritical crack-growth under sustained load in Ti-6Al-6V-2Sn. *Metallurgical Transactions A*, 12(1):83–94, Jan 1981. ISSN 1543-1940. doi:10.1007/BF02648512.
- [34] J. S. Nadeau. Subcritical crack growth in vitreous carbon at room temperature. *Journal of the American Ceramic Society*, 57(7):303–306, 1974. doi:10.1111/j.1151-2916.1974.tb10906.x.
- [35] George B. Kaufman. Inorganic chemistry: principles of structure and reactivity, 4th ed. *Journal of Chemical Education*, 70(10):A279, 1993. doi:10.1021/ed070pA279.1.

- [36] D.S. Dugdale. Yielding of steel sheets containing slits. *Journal of the Mechanics and Physics of Solids*, 8(2): 100 – 104, 1960. ISSN 0022-5096. doi:10.1016/0022-5096(60)90013-2.
- [37] K. T. Tallakstad, R. Toussaint, S. Santucci, J. Schmittbuhl, and K. J. Måløy. Local dynamics of a randomly pinned crack front during creep and forced propagation: An experimental study. *Phys. Rev. E*, 83:046108, 04 2011.
- [38] A. Cochard, O. Lengliné, K. J. Måløy, and R. Toussaint. Thermally activated crack fronts propagating in pinning disorder: simultaneous brittle/creep behavior depending on scale. *Philosophical Transactions of the Royal Society A : Mathematical, Physical and Engineering Sciences*, 2018. doi:10.1098/rsta.2017.0399.
- [39] D. W. Tang and N. Araki. On non-fourier temperature wave and thermal relaxation time. *International Journal of Thermophysics*, 18(2):493, Mar 1997. ISSN 1572-9567. doi:10.1007/BF02575178.
- [40] C. L. Rountree, Rajiv K. K., E. Lidorikis, A. Nakano, L. Van Brutzel, and P. Vashishta. Atomistic aspects of crack propagation in brittle materials: Multimillion atom molecular dynamics simulations. *Annual Review of Materials Research*, 32(1):377–400, 2002. doi:10.1146/annurev.matsci.32.111201.142017.
- [41] Y. Hwangbo, C-K. Lee, S-M. Kim, J-H. Kim, K-S. Kim, B. Jang, H-J. Lee, S-K. Lee, S.S. Kim, J-H. Ahn, and S-M. Lee. Fracture characteristics of monolayer cvd-graphene. *Scientific Reports*, 4:4439, 03 2014. doi:10.1038/srep04439.
- [42] A. Balandin, S. Ghosh, W. Bao, I. Calizo, D. Teweldebrhan, F. Miao, and J. Lau. Superior thermal conductivity of single-layer graphene. *Nano letters*, 8:902–7, 04 2008. doi:10.1021/nl0731872.
- [43] X. Huang, G. Liu, and X. Wang. New secrets of spider silk: Exceptionally high thermal conductivity and its abnormal change under stretching. *Advanced Materials*, 24(11):1482–1486, 2012. doi:10.1002/adma.201104668.
- [44] J. R. Rice. Heating and weakening of faults during earthquake slip. *Journal of Geophysical Research: Solid Earth*, 111(B5), 2006. doi:10.1029/2005JB004006.
- [45] Germán A. Prieto, Manuel Florez, Sarah A. Barrett, Gregory C. Beroza, Patricia Pedraza, Jose Faustino Blanco, and Esteban Poveda. Seismic evidence for thermal runaway during intermediate-depth earthquake rupture. *Geophysical Research Letters*, 40(23):6064–6068, 2013. doi:10.1002/2013GL058109.
- [46] C. H. Scholz. The brittle-plastic transition and the depth of seismic faulting. *Geologische Rundschau*, 77(1):319–328, Feb 1988. ISSN 1432-1149. doi:10.1007/BF01848693.
- [47] E. Aharonov and C. H. Scholz. The brittle-ductile transition predicted by a physics-based friction law. *Journal of Geophysical Research: Solid Earth*, 124(3):2721–2737, 2019. doi:10.1029/2018JB016878.

Is breaking through matter a hot matter? A material failure prediction by monitoring creep

SUPPLEMENTARY MATERIAL

Tom Vincent-Dospital,^{1,2,*} Renaud Toussaint,^{1,2,†} Alain Cochard,¹ Eirik G. Flekkøy,² and Knut Jørgen Måløy²

¹*Université de Strasbourg, CNRS, IPGS UMR 7516, F-67000 Strasbourg, France*

²*SFF Porelab, The Njord Centre, Department of physics, University of Oslo, Norway*
(Dated: August 2, 2022)

CONTENTS

I. Analytical approximation of the avalanche threshold	1
II. The arrest threshold (for completeness)	2
III. Materials creep crossplots and parameters table	3
References	7

I. ANALYTICAL APPROXIMATION OF THE AVALANCHE THRESHOLD

Let us start this additional material with the analytical approximations of the temperature at a running crack tip. Assuming a quasi-constant velocity and energy release rate, some simplified expressions can indeed be derived [1] for ΔT . At low velocity, the typical diffusion skin depth is large compared to the radius of the heat production zone ($\sqrt{\lambda l / (V \pi C)} / l \gg 1$) and the heat diffusion is hence the ruling process:

$$\Delta T_{\text{slow}} \sim \phi G \frac{V}{\lambda}. \quad (1)$$

At high velocity, however, the rise in temperature is limited by the scale over which heat is produced and:

$$\Delta T_{\text{fast}} \sim \frac{\phi G}{\pi C l}. \quad (2)$$

Between these two cases, and typically for $V \sim \lambda / (\pi C l)$, an intermediate regime holds:

$$\Delta T_{\text{mid}} \sim \phi G \sqrt{\frac{V}{4\pi C \lambda l}}. \quad (3)$$

We invite the reader to a more in-depth derivation of these equations in Toussaint et al. [1] or Vincent-Dospital et al. [2].

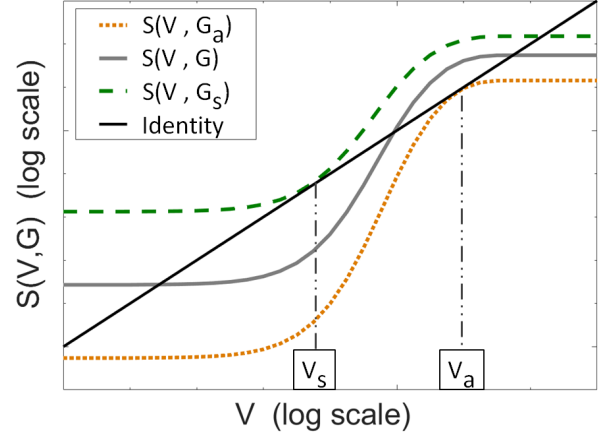


FIG. 1. Representation of $V = S(V, G)$ for three values of G : G_s , G_a and a mid-value between G_s and G_a (plain plot). The intersections of S_G with the identity plot (straight line) give the possible crack velocities for a given energy release rate, as per Eq. (4). The axes are not annotated for the sake of generality. See Ref. [2] for further information.

Now that some straightforward expressions for ΔT are known, we can move on to infer G_a . Our model, the Arrhenius law as considered in the main manuscript, defines a function $S(V, G)$ such that $S(V, G) = V$:

$$S(V, G) = V_0 \min \left[\exp \left(- \frac{\alpha^2 [G_c - G]}{k_B [T_0 + \Delta T(V, G)]} \right), 1 \right]. \quad (4)$$

To lighten the equations that will follow, we have here denoted α^2 the ratio $d_0^3 / (2l)$. We have discussed, in the main manuscript, how this relation might have one to three solutions depending on G (see Fig. 1). Two particular energy release rates mark the passages from a singular to multiple solutions: the avalanche threshold G_a , of interest in this study, and another threshold, G_s , which is the load at which an avalanche has to stop.

All functions being continuously smooth, the switch from one solution to three solutions implies that $S(V, G)$ is tangent to the identity function for these two particular G , as illustrated in Fig 1. G_a and the corresponding velocity V_a must therefore verify the following system of equations:

* vincentdospital@unistra.fr

† renaud.toussaint@unistra.fr

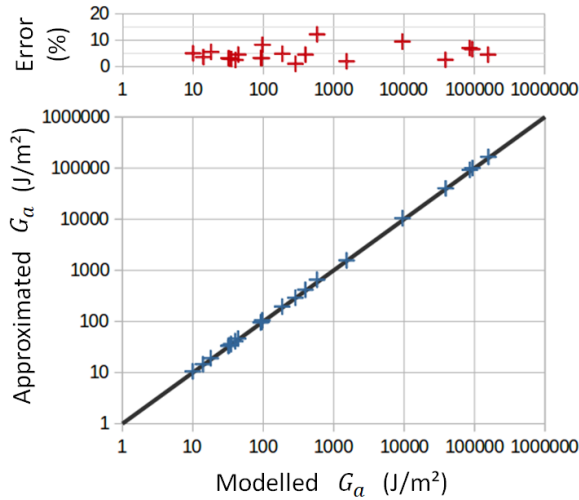


FIG. 2. (Bottom): G_a threshold, as approximated by Eq. (11) versus the accurate numerical solution of the model. The black line is the identity. (Top): Relative error from the approximation

$$S(V, G) = V \quad (5)$$

$$\frac{\partial S}{\partial V}(V, G) = 1. \quad (6)$$

To solve this system, we assume that the transition towards the fast phase happens in a regime where the temperature elevation still increases linearly with the crack velocity (i.e., $\Delta T = \Delta T_{\text{slow}}(V, G)$ (1)). Equation (6) then becomes:

$$\frac{\phi G \lambda \alpha^2 (G_c - G)}{k_b (\lambda T_0 + \phi G V)^2} S(V, G) = 1. \quad (7)$$

Inserting Eq. (5) back into (7) leads to the following quadratic equation in V :

$$\left(\frac{\phi G V}{\lambda T_0} \right)^2 + \left[2 + \frac{\alpha^2 (G - G_c)}{k_b T_0} \right] \frac{\phi G V}{\lambda T_0} + 1 = 0. \quad (8)$$

While it might of course hold two solutions, only the lower one is of interest to derive the avalanche threshold G_a . The upper solution would indeed correspond to the ‘arrest’ of the crack avalanche, but the initial hypothesis of $\Delta T = \Delta T_{\text{slow}}$ would there anyway be wrong, as this ‘arrest’ occurs while on the quick (hot) propagation branch. Focusing therefore on the lower solution of (8), we have:

$$V_a = \frac{T_0 \lambda}{2\phi G_a} (R_a - 2 - R_a \sqrt{1 - 4/R_a}), \quad (9)$$

with $R_a = \alpha^2 (G_c - G_a) / (k_B T_0)$. This equation indicates at which slow velocity a crack avalanches, given

the corresponding G_a threshold. Substituting (9) in (5), one finally derives the equality that defines the avalanche threshold:

$$G_a \sim \frac{\lambda T_0}{2\phi V_0} \frac{R_a - 2 - R_a \sqrt{1 - 4/R_a}}{\exp\left(-2/[1 - \sqrt{1 - 4/R_a}]\right)}. \quad (10)$$

Such an expression gives a fairly good approximation of G_a as predicted by the model. The only hypothesis was indeed the validity of Eq. (1), that is $\sqrt{\lambda l / (V_a \pi C)} / l \gg 1$ and, for the materials that we have studied in our manuscript, this ratio ranges from 300 to 1500. While Eq. (10) is easy to solve for G_a with any numerical method, it can however be further simplified by grossly assuming that $R_a \gg 4$ and by developing the term $\sqrt{1 - 4/R_a}$. We thus obtain the equation presented in the manuscript:

$$G_a \sim \frac{\lambda T_0}{\phi V_0} \frac{\exp(R_a)}{R_a}. \quad (11)$$

Figure 2 shows the quality of the approximation for G_a , off by a few percents as, as shown in Tab. I, the $R_a \gg 4$ hypothesis is not strictly valid.

II. THE ARREST THRESHOLD (FOR COMPLETENESS)

Similarly, one can solve (5) and (6) at the ‘arrest’ point: the transition from a quick regime back to the low velocity phase, occurring at the particular load G_s . While G_a is vastly reported for a lot of materials, making it the topic of this manuscript, G_s is more rarely reported, so that the following computation is given for completeness. We here assume that the transition arises when the crack cools down from the plateau temperature $\Delta T = \Delta T_{\text{fast}}(G)$ (2), along the intermediate slope defined by $\partial \Delta T / \partial V = \partial \Delta T_{\text{mid}}(V, G) / \partial V$ (3). We thus turn the system into a quadratic equation of \sqrt{V} :

$$\left(\frac{\phi G \sqrt{V}}{4\pi \lambda C l T_0} \right)^2 + \left(2 + \frac{\alpha^2 (G - G_c)}{2k_b T_0} \right) \left(\frac{\phi G \sqrt{V}}{4\pi \lambda C l T_0} \right) + 1 = 0, \quad (12)$$

the upper solution of which, together with Eq. (5), leads to:

$$V_s = \frac{\pi \lambda C l T_0^2}{4(\phi G_s)^2} \left[R_s - 4 + R_s \sqrt{1 - 8/R_s} \right]^2, \quad (13)$$

where $R_s = \alpha^2 (G_c - G_s) / (k_B T_0)$. When inserting (13) back into (5), one gets:

$$\frac{4(\phi G_s)^2 V_0}{\pi \lambda C l T_0^2} = \frac{\left[R_s - 4 + R_s \sqrt{1 - 8/R_s} \right]^2}{\exp\left(\frac{\alpha^2(G_s - G_c)}{k_b[T_0 + \phi G_s/(\pi C l)]}\right)}. \quad (14)$$

Assuming that $R_s \gg 8$ and $\Delta T_{\text{fast}} \gg T_0$, Eq. (14) further simplifies to:

$$G_s \sim \frac{T_0}{\phi} \sqrt{\frac{\pi C l}{V_0}} \exp\left(\frac{\pi C l T_0}{2\phi G_s}\right) R_s, \quad (15)$$

which gives a relatively simple expression to invert for G_s .

III. MATERIALS CREEP CROSSPLOTS AND PARAMETERS TABLE

A summary of the model parameters considered for each media is also provided in Tab. I. These parameters are deduced, as explained in the main manuscript, from the V to G creep data of these materials, shown in Fig 3 to Fig 20. One can notably notice the variability in fit quality for these datasets, that of course impacts our inversion work, but also how it is not always straight forward to know to which subcritical phase the data correspond (i.e., phase I to III, from environmental induced corrosion to void-like conditions).

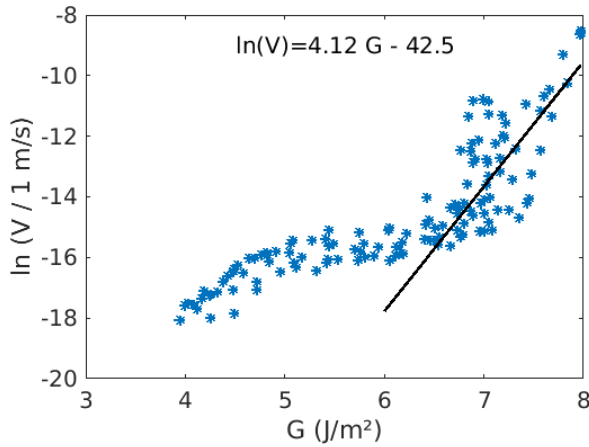


FIG. 3. Creep data of dry soda-lime glass, from Wiederhorn [3], figure 3. A rather complex creep law holds there so that we only roughly fitted the last part.

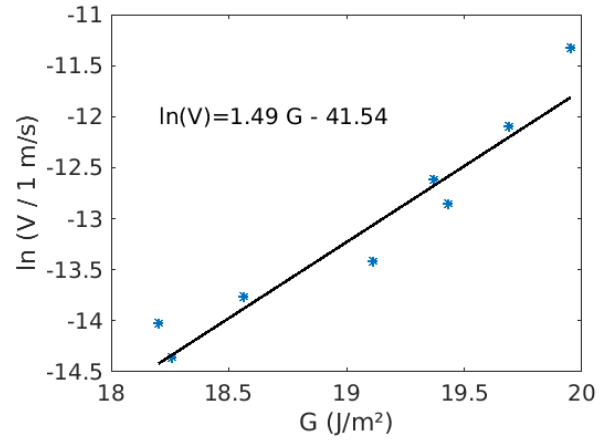


FIG. 4. Creep data of dry sapphire (r-plane), from Wiederhorn and Krause [4].

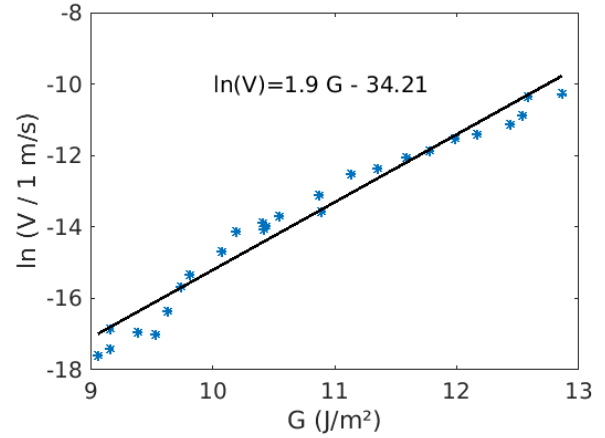


FIG. 5. Creep data of quartz in vacuum, from Dove [5], figure 4.

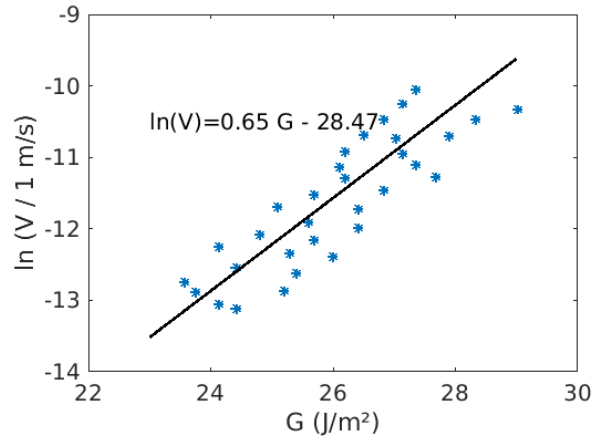


FIG. 6. Creep data of Scioto sandstone, from Holder et al. [6], figure 3.

	λ (SI)	ϕ (-)	V_0 (m/s)	l (Å)	T_0 (K)	G_c (J/m ²)	G_a real (J/m ²)	G_a model (J/m ²)	Ra (-)
Acrylic adhesive	0.4	1	30	10	296	150	90	97	5.7
Paper	0.035	0.12	1300	1000	296	25000	14000	9500	15.6
Bulk PMMA	0.18	0.2	880	80	296	1300	700	580	10.9
Interfacial PMMA	0.18	0.2	880	8	298	275	140	190	13.5
HD Polyethylene	0.4	0.5	900	8500	293	200000	70000	87000	16.6
Soda lime glass	1	0.5	3400	0.3	296	12	8	10	8.3
Sapphire	24	0.5	6000	0.8	296	36	20	32	6
Quartz	8	0.5	3400	0.6	293	21	13	18	5.7
Westerly Granite (ambient)	2	0.5	3000	4	293	120	68	92	8.5
Westerly Granite (hot)	2	0.5	3000	0.7	573	43	24	35	6.8
Kumamoto Andesite	1	0.5	2200	3	330	120	80	97	8.8
Scioto Sandstone	2	0.5	2000	2	296	55	37	44	7.3
Cement paste	1	0.5	2200	3	298	310	250	280	10.7
HSULP Concrete	0.8	0.5	3000	1	293	44	38	40	9.9
Vitreous carbon	5	0.5	2600	0.2	296	15	13	14	7.2
Lead Zirconate Titanate (PZT)	1	0.5	2000	1	296	40	24	33	11.3
Tetragonal zirconia (TZP)	2	0.5	1600	40	298	1900	1500	1530	10.9
Silicon nitride	30	0.5	5500	45	1573	510	260	400	8.9
2650 T6 Aluminium alloy	150	0.5	3100	1000	448	54500	27000	39000	10.1
AISI 310S Stainless Steel alloy	14	0.5	3000	9000	298	265000	102000	158000	13.4
Ti-6Al-6V-2Sn Titanium	7	0.5	3100	8000	298	190000	72000	93000	14.9

TABLE I. Model parameters for various materials of the literature. The real and modelled G_a thresholds are compared in the two former last columns. The cells colour help to highlight standing out values for λ and T_0 .

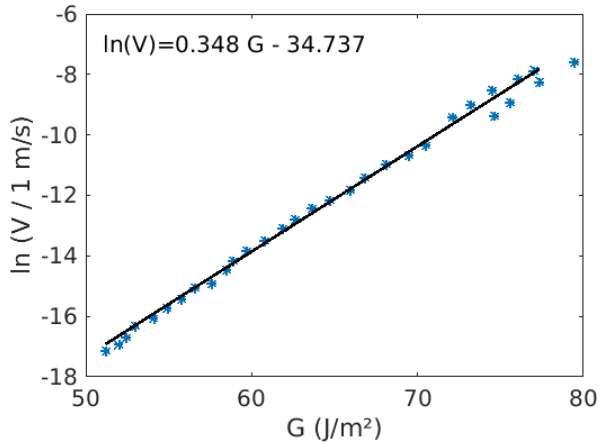


FIG. 7. Creep data of Kumamoto andesite in moist air at 67 °C, from Nara and Kaneko [7], figure 9.

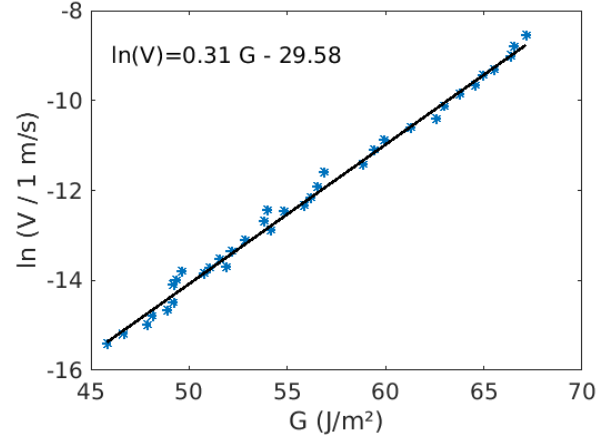


FIG. 8. Creep data of Westerly granite in moist air at 20 °C, from Meredith and Atkinson [8], figure 7.

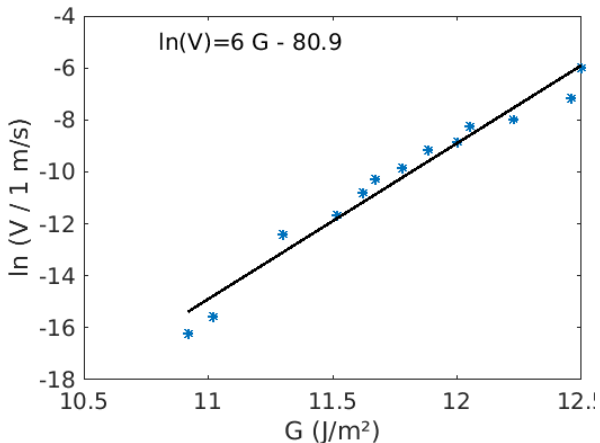


FIG. 9. Creep data of vitreous carbon, from Nadeau [9], figure 4.

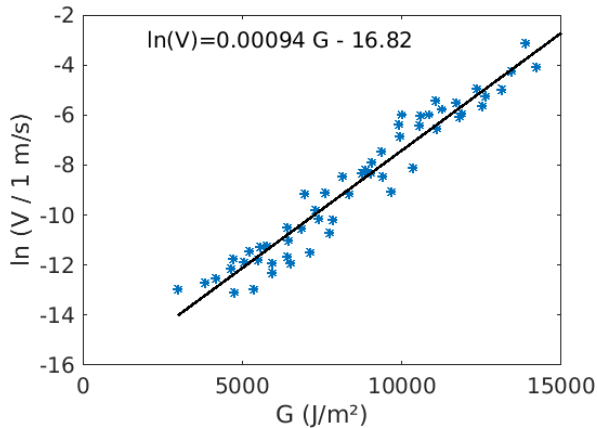


FIG. 12. Creep data of paper in air, from Santucci [12], figure 3.32.

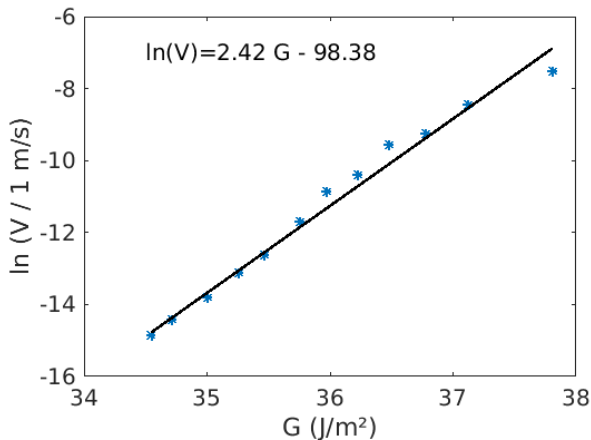


FIG. 10. Creep data of high strength ultra low porosity concrete in moist air, from Nara et al. [10], figure 9.

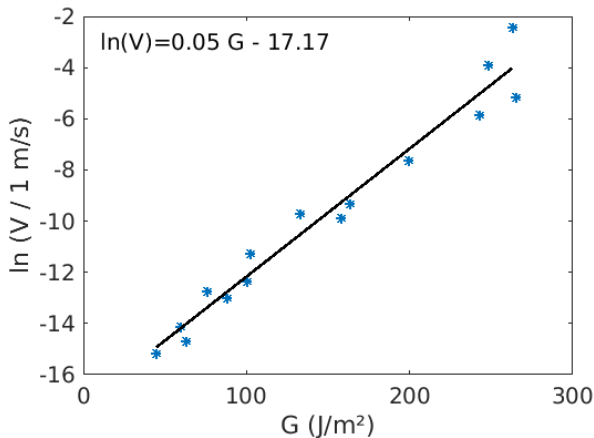


FIG. 13. Creep data of hot silicon nitride at 1200 °C, from Evans and Wiederhorn [13], figure 5.

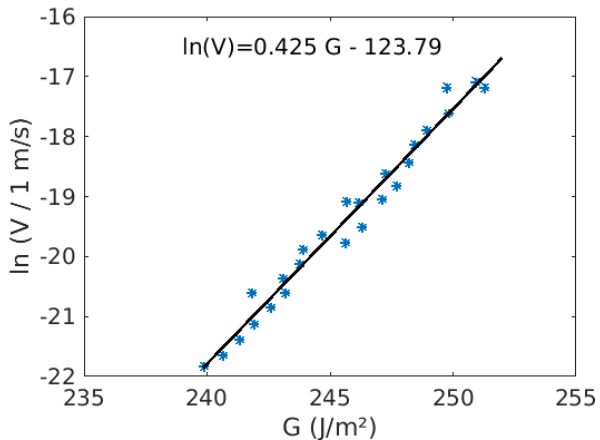


FIG. 11. Creep data cement in water, from Wang et al. [11], figure 4a.

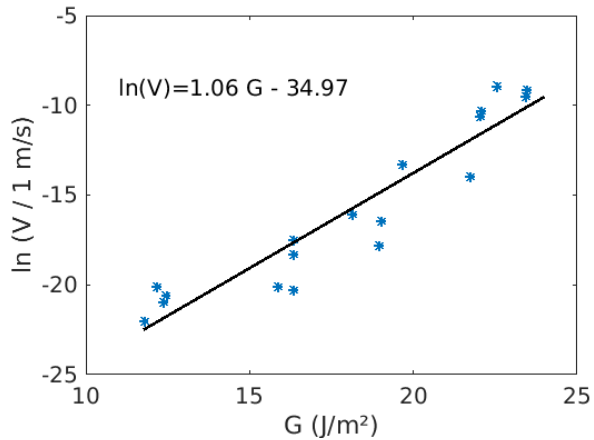


FIG. 14. Creep data of Lead Zirconate Titanate at ambient conditions, from Oates et al. [14], figure 2 (open circuit).

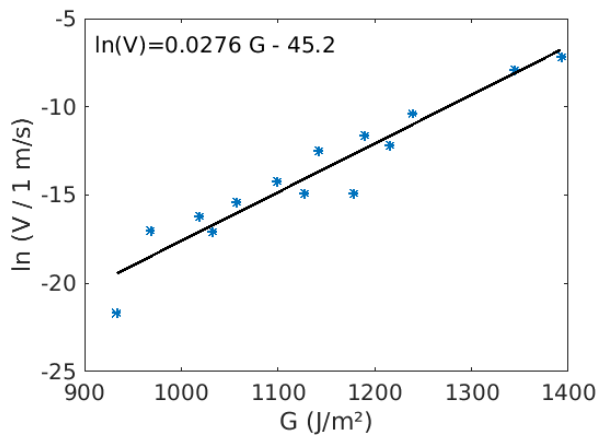


FIG. 15. Creep data tetragonal zirconia (TZP) in vacuum, from Chevalier et al. [15], figure 5.

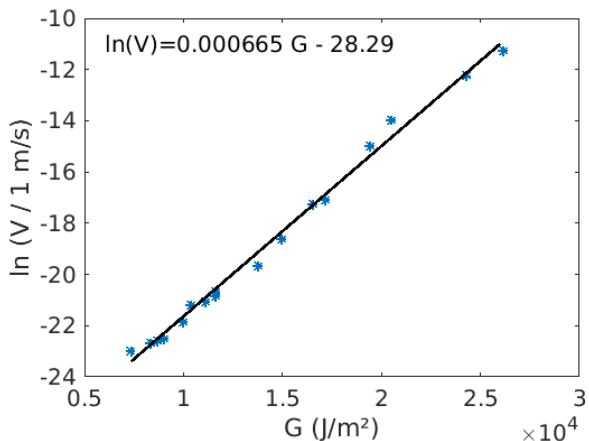


FIG. 18. Creep data of aluminium 2650 T6 alloy in vacuum at 175 °C, from Hénaff et al. [18], figure 6.

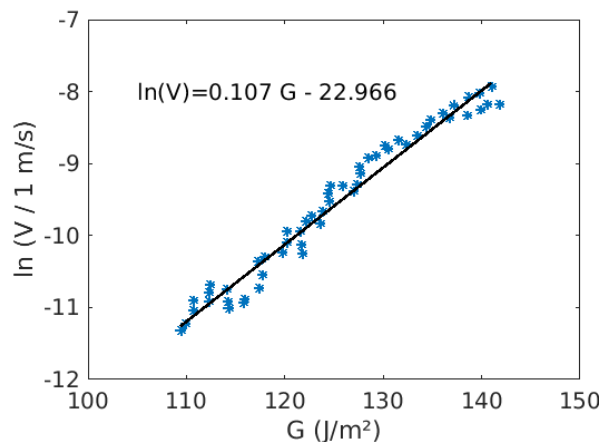


FIG. 16. Interfacial creep data in sintered PMMA plates in air, from Lengliné et al. [16], figure 5.

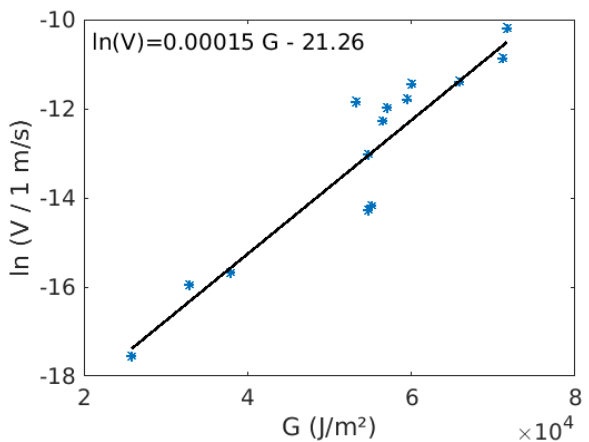


FIG. 19. Creep data in Ti-6Al-6V-2Sn titanium alloy in moist air, from Sastry et al. [19], figure 6a (beta annealed).

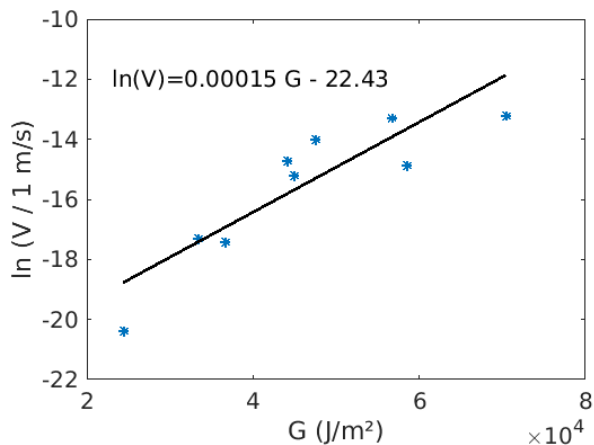


FIG. 17. Creep data of high density polyethylene, from Yoda et al. [17], figure 4.

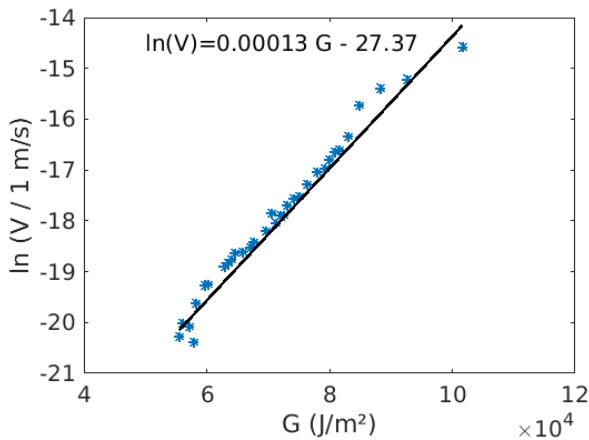


FIG. 20. Creep data of AISI 310S austenitic stainless steel in air, from Huang and Altstetter [20], figure 1 (uncharged plot).

-
- [1] R. Toussaint, O. Lengliné, S. Santucci, T. Vincent-Dospital, M. Naert-Guillot, and K. J. Måløy. How cracks are hot and cool: a burning issue for paper. *Soft Matter*, 12:5563–5571, 2016. doi:10.1039/C6SM00615A.
- [2] T. Vincent-Dospital, R. Toussaint, A. Cochard, K. J. Måløy, and E. G. Flekkøy. Thermal weakening of cracks, a phase transition model. submitted, 2018. URL <https://arxiv.org/pdf/1901.04202.pdf>.
- [3] S. M. Wiederhorn. Influence of water vapor on crack propagation in soda-lime glass. *Journal of the American Ceramic Society*, 50(8):407–414, 1967. doi:10.1111/j.1151-2916.1967.tb15145.x.
- [4] S.M. Wiederhorn and R.F. Jr. Krause. Crack growth in sapphire. In *Ceramic Engineering and Science Proceedings*, volume 23, pages 71–82. Wiley, 2002.
- [5] P. M. Dove. Geochemical controls on the kinetics of quartz fracture at subcritical tensile stresses. *Journal of Geophysical Research: Solid Earth*, 100(B11):22349–22359, 1995. doi:10.1029/95JB02155.
- [6] J. Holder, J. E. Olson, and Z. Philip. Experimental determination of subcritical crack growth parameters in sedimentary rock. *Geophysical Research Letters*, 28(4):599–602, 2001. doi:10.1029/2000GL011918.
- [7] Y. Nara and K. Kaneko. Study of subcritical crack growth in andesite using the double torsion test. *International Journal of Rock Mechanics and Mining Sciences*, 42(4):521 – 530, 2005. ISSN 1365-1609. doi:10.1016/j.ijrmms.2005.02.001.
- [8] P.G. Meredith and B.K. Atkinson. Fracture toughness and subcritical crack growth during high-temperature tensile deformation of westerly granite and black gabbro. *Physics of the Earth and Planetary Interiors*, 39(1):33 – 51, 1985. ISSN 0031-9201. doi:10.1016/0031-9201(85)90113-X.
- [9] J. S. Nadeau. Subcritical crack growth in vitreous carbon at room temperature. *Journal of the American Ceramic Society*, 57(7):303–306, 1974. doi:10.1111/j.1151-2916.1974.tb10906.x.
- [10] Y. Nara, M. Takada, D. Mori, H. Owada, T. Yoneda, and K. Kaneko. Subcritical crack growth and long-term strength in rock and cementitious material. *International Journal of Fracture*, 164(1):57–71, Jul 2010. ISSN 1573-2673. doi:10.1007/s10704-010-9455-z.
- [11] W. Wang, T. Tong, and Q. Yu. Subcritical crack growth induced by stress corrosion in hardened cement paste. In *9th International Conference on Fracture Mechanics of Concrete and Concrete Structures*. FraMCoS, 2016. doi:10.21012/FC9.177.
- [12] S. Santucci. *Croissance lente thermiquement activée et piégeage d’une fissure dans les matériaux structurés à une échelle mésoscopique : expériences et modèles*. PhD thesis, Ecole normale supérieure de Lyon, www.theses.fr/2004ENSL0288, 2004.
- [13] A. G. Evans and S. M. Wiederhorn. Crack propagation and failure prediction in silicon nitride at elevated temperatures. *Journal of Materials Science*, 9(2):270–278, Feb 1974. ISSN 1573-4803. doi:10.1007/BF00550951.
- [14] W. S. Oates, C. S. Lynch, D. C. Lupascu, A. B. K. Njiwa, E. Aulbach, and J. Rödel. Subcritical crack growth in lead zirconate titanate. *Journal of the American Ceramic Society*, 87(7):1362–1364, 2004. doi:10.1111/j.1151-2916.2004.tb07736.x.
- [15] J. Chevalier, C. Olagnon, and G. Fantozzi. Subcritical crack propagation in 3Y-TZP ceramics: Static and cyclic fatigue. *Journal of the American Ceramic Society*, 82(11):3129–3138, 1999. doi:10.1111/j.1151-2916.1999.tb02213.x.
- [16] O. Lengliné, R. Toussaint, J. Schmittbuhl, J. E. Elkhoury, J. P. Ampuero, K. T. Tallakstad, S. Santucci, and K. J. Måløy. Average crack-front velocity during subcritical fracture propagation in a heterogeneous medium. *Phys. Rev. E*, 84:036104, Sep 2011. doi:10.1103/PhysRevE.84.036104.
- [17] M. Yoda, M. Nabetani, and W. Shim. Creep crack growth in polyethylene under combined mode I and mode II loading. *International Journal of Fracture*, 112(3):21–26, Dec 2001. ISSN 1573-2673. doi:10.1023/A:1022681718523.
- [18] G. Hénaff, G. Odemer, and B. Journet. Creep and creep-fatigue crack growth in aluminium alloys. In *Aluminium Alloys, Theory and Applications*, pages 259–282. IntechOpen, 2011. doi:10.5772/15153.
- [19] S. M. L. Sastry, R. J. Lederich, and B. B. Rath. Subcritical crack-growth under sustained load in Ti-6Al-6V-2Sn. *Metallurgical Transactions A*, 12(1):83–94, Jan 1981. ISSN 1543-1940. doi:10.1007/BF02648512.
- [20] J. H. Huang and C. J. Altstetter. Internal hydrogen-induced subcritical crack growth in austenitic stainless steels. *Metallurgical Transactions A*, 22(11):2605–2618, Nov 1991. ISSN 1543-1940. doi:10.1007/BF02851354.